AIAA JOURNAL
Vol. 42, No. 10, October 2004

Aero-Optical Wavefronts and Scale-Local Characterization in Large-Reynolds-Number Compressible Turbulence

Roberto C. Aguirre* and Haris J. Catrakis†
University of California, Irvine, Irvine, California 92697

A new technique is proposed that enables the scale-local characterization of aero-optical wavefronts. Because optical wavefronts degraded by turbulent flows are physically highly anisotropic and exhibit distortions over a wide range of scales, a method is needed to examine the wavefront structure at varying degrees of anisotropy and as a function of scale. We introduce an aero-optical-wavefront-anisotropy (AWA) parameter as the ratio of scaling factors for the wavefront distortions and for the wavefront transverse extent. This AWA parameter, combined with box counting, enables a scale-local anisotropic examination of the wavefronts. We demonstrate this technique on wavefronts derived from experiments on large-Reynolds-number ($Re \sim 10^6$) high-compressibility ($M_c \sim 1$) turbulent shear layers between dissimilar-index-of-refraction gases. Variation of the AWA parameter and scale-local examination of the distortions reveal the presence of anisotropic self-similarity, or self-affinity, at small scales spanning nearly a decade. This finding shows the utility of the technique to detect scaling in large-Reynolds-number flow experiments from the aero-optical behavior. The present finding and technique provide key ingredients to extrapolate the small-scale properties of compressible-flow aero-optical wavefronts to higher Reynolds numbers and are also useful for modeling and for computational aero-optics.

I. Introduction

AIRBORNE applications requiring long-range directed-energy propagation or high-resolution optical imaging involve flows necessarily associated with large Reynolds numbers and require knowledge of both the large-scale and small-scale behavior for a complete description. Practically, quantifying the relative contributions of the large-scale vs small-scale properties is helpful for the improvement of techniques to optimize performance in applications ranging from free-space communication systems (e.g., Ref. 1) to high-energy airborne lasers as well as atmospheric-observation airborne platforms (e.g., Ref. 2). Aero-optical distortions in subsonic flows can arise from at least two different mechanisms depending on whether the flow involves total-temperature-matched airstreams, in which case the distortions are largely caused by fluid dynamic and thermodynamic effects of flow curvature and velocity fluctuations,[3,4] or dissimilar gases with different refractive indices in which case the distortions are dominated by the mixing process.[5] In supersonic flows, additional mechanisms are present in both cases as a result of optical distortions associated with compression and expansion waves. The differences in the aero-optical mechanisms between the case of total-temperature-matched airstreams and the case of dissimilar gases are significant, as emphasized by Jumper and Fitzgerald[6] and also discussed in the companion article to the present work.[7] With regard to Reynolds-number effects, at a given Mach number and for a given flow geometry, it can be appreciated that the number of small-scale features increases with increasing Reynolds number, and this needs to be taken into account when comparing large-scale effects to the aggregate small-scale effects on optical distortions at large Reynolds numbers. Although the large-scale properties of aero-optical interactions in turbulent flows can be expected to be strongly dependent on the flow geometry and boundary conditions (e.g., Refs. 2, 4, 5, 6, and 8–10), the small-scale properties behave quite differently. At least at large Reynolds numbers and for incompressible flow conditions, there is evidence that the small-scale flow structure can exhibit scale-local self-similarity or scaling (e.g., Refs. 11 and 12), and this can be expected to be at most weakly sensitive to the flow geometry. Small-scale turbulence statistics appear to be independent of the flow geometry or large-scale behavior to a good approximation, as long as the Reynolds number is sufficiently large for the turbulent behavior to be fully developed. This requires at a minimum that the Reynolds number Re based on the large scales must be at least $Re \gtrsim 10^4$ (e.g., Ref. 13).

A useful point of view for developing techniques to characterize highly irregular optical or fluid-mechanical objects, such as turbulence-aberrated optical wavefronts or turbulence-generated fluid interfaces, is to examine geometrical properties as a function of scale (e.g., Ref. 14 and references therein) and particularly the extent to which self-similar/fractal behavior (e.g., Refs. 11 and 15) or scale-dependent behavior (e.g., Ref. 16) is exhibited at the small scales. Because the structure of aero-optical wavefronts is essentially determined by the turbulent flow structure, one can expect that the aero-optical distortions will exhibit self-similar behavior at small scales if the refractive fluid interfaces are self-similar. This has been suggested theoretically for optical wavefronts distorted by incompressible turbulent flows (e.g., Refs. 17–19). For compressible flows, there is some evidence that the small-scale structure of fluid interfaces can exhibit self-similarity (e.g., unpublished work of Sreenivasan and Johnson cited in Smits and Dussauge[20] and Poggie[21]). Such self-similarity can expected to be at most weakly dependent on the large-scale flow properties. Thus, for compressible turbulence, one might expect self-similar scaling behavior for the small-scale properties of both the turbulent fluid interfaces and the turbulence-distorted optical wavefronts. Self-similar behavior of the optical wavefronts, if found at high compressibility, would permit extrapolating the small-scale optical behavior to the large Reynolds numbers of interest in practical applications in high-speed flight.

In the present work, we introduce an aero-optical-wavefront-anisotropy (AWA) parameter defined as a ratio of scaling factors for the optical path difference (OPD) and for the wavefront spatial extent. This is described in Sec. II in the context of the physical anisotropy of aero-optical wavefronts. The AWA parameter enables the examination of the small-scale geometrical properties of

Presented as Paper 2002-2269 at the AIAA 33rd Plasmadynamics and Lasers Conference, Maui, HI, 20–23 May 2002; received 21 January 2003; revision received 7 May 2004; accepted for publication 7 May 2004.

*Graduate Student, Aeronautics and Fluid Dynamics Laboratories, Mechanical and Aerospace Engineering, Henry Samueli School of Engineering. Member AIAA.

†Assistant Professor, Aeronautics and Fluid Dynamics Laboratories, Mechanical and Aerospace Engineering, Henry Samueli School of Engineering; catrakis@uci.edu. Member AIAA.

the wavefronts using an anisotropic extension of the box counting method, and this is developed in Sec. III. We demonstrate the utility of this technique on wavefront data derived from large-Reynolds-number high-compressibility shear layers between optically different gases. A description of the experimental technique, and a discussion of the important issue of mixing vs density effects in aero-optics, can be found in the companion paper[7] and references therein. In Sec. IV the results of the scale-local examination of the wavefront data are presented. The AWA parameter is found to be useful to discern anisotropically self-similar, or self-affine, behavior of the OPD at small scales. This scaling behavior can be expected in other large-Reynolds-number, highly compressible flows because the small-scale behavior is at most weakly dependent on the large-scale behavior, as long as the Reynolds number is large enough for the turbulent flow to be fully developed. Consequences of the present findings are discussed, in the conclusions, regarding large-Reynolds-number experimental studies, modeling, and computational aero-optics. Considerations of the large-scale aero-optical distortions, using a new interfacial-fluid-thickness approach, are the subject of the companion paper.[7]

II. AWA Parameter in Large-Reynolds-Number Turbulent Flows

One of the practical as well as fundamental objectives in aero-optics is to develop the means to extrapolate the behavior of the optical-wavefront structure to larger Reynolds numbers, including effects of compressibility. Knowledge of the small-scale structure of aero-optical wavefronts is needed toward this objective. Optical wavefronts propagating through turbulent flows can be expected to exhibit behavior that is similar to, or related closely to, the flow structure. To be able to extrapolate the behavior of a turbulence-generated refractive-index field $n(\boldsymbol{x}, t)$ to large Reynolds numbers, it is important that the Reynolds number of the flow under study be at least above the minimum value associated with the transition to fully developed turbulence (e.g., Ref. 13), i.e.,

$$Re \gtrsim 10^4 \tag{1}$$

As long as the turbulent flow is fully developed, that is, satisfies at least the criterion in Eq. (1), the range of scales exhibited by the refractive field $n(\boldsymbol{x}, t)$ increases with increasing Reynolds number, as is well known, as

$$\lambda_{\max}/\lambda_{\min} \sim Re^{\frac{3}{4}} \tag{2}$$

for gas-phase flows,[22] where $\lambda_{\min}$ is the smallest scale or Kolmogorov scale and $\lambda_{\max}$ is the largest scale identified as the extent of the flow region through which the wavefronts propagate or alternatively as the extent of large-scale shear in the flow. An important issue, in the context of the present work, is that there is a narrower range of scales, which appears for large-Reynolds-number flows and refractive-index fields, and this is the range of scales bounded from above by the Liepmann–Taylor scale λ_{LT} and from below by $\lambda_{\min}$, that is,

$$\lambda_{\min} \lesssim \lambda \lesssim \lambda_{\mathrm{LT}} \sim \lambda_{\max} Re^{-\frac{1}{2}} \tag{3}$$

where similarity properties (e.g., Ref. 22), including possibly self-similarity (e.g., Ref. 11), are present. The Liepmann–Taylor scale λ_{LT} denotes the largest of the small scales that are not directly affected by large-scale effects or, equivalently, the smallest scale that is directly affected by large-scale effects. Such properties are important because they can be expected to help extrapolate aero-optical behavior to larger Reynolds numbers, encountered in practice, in both incompressible and compressible flows (e.g., Ref. 20).

A schematic showing a planar wavefront incident on a three-dimensional optically active turbulent-flow region and the irregular wavefront emerging from the flow in three dimensions is depicted in Fig. 1. To characterize aero-optical distortions over the wide range of scales associated with large values of the Reynolds number [compare Eqs. (1–3)], techniques are needed that enable the description of optical-wavefront structure as a function of scale.

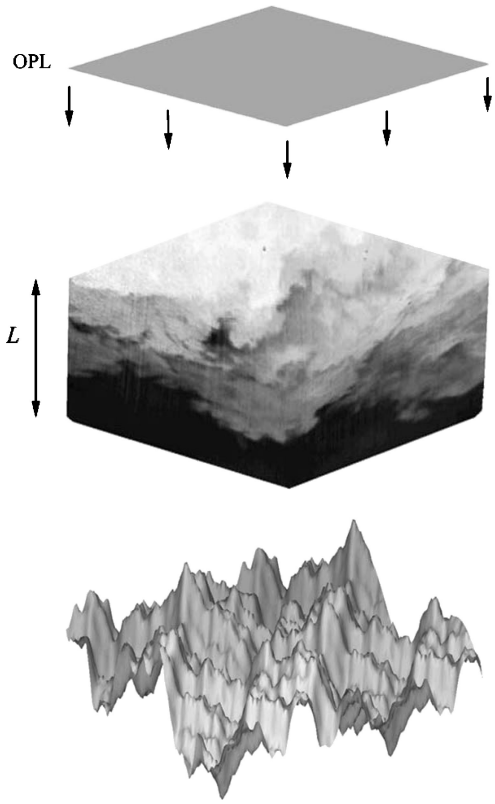

Fig. 1 Schematic of a planar optical wavefront (top) incident to a three-dimensional refractive-index field in a large-Reynolds-number turbulent compressible flow (middle), and the emerging highly irregular aero-optical wavefront (bottom).

Most previous studies of the small-scale flow behavior and of the optical-wavefront behavior have focused on spectral descriptions or, equivalently, on descriptions based on second-order structure functions (e.g., Refs. 5 and 23). Spectral descriptions, however, characterize the aero-optical behavior in Fourier space and do not uniquely identify the geometrical structure of the turbulent flow or optical wavefronts. This is because power spectra retain no phase information. The description of the geometrical structure of turbulent flows in physical space is a relatively recent development (e.g., Refs. 11 and 12) and relies on box-counting techniques. A generalized version of the box-counting technique, which can characterize anisotropic surfaces such as optical wavefronts, will be proposed and described in Sec. III. In the present section, the issue of optical-wavefront anisotropy will be first addressed as it is a crucial physical aspect of wavefront structure and an important ingredient of the new box-counting technique of Sec. III.

The governing equation for the propagation of optical wavefronts, at the level of description of geometrical optics, is the eikonal equation

$$|\nabla(\mathrm{OPL})| = n \tag{4}$$

for the optical path length (OPL), or, equivalently, the inverse solution to the eikonal equation, which is the integral for the OPL in terms of the refractive index along the optical beam propagation path, that is,

$$\mathrm{OPL}(\boldsymbol{x}, t) \equiv \int_{\mathrm{ray}} n(\ell, t)\, \mathrm{d}\ell \equiv \int_{\mathrm{ray}} n(\ell, t) h_{n,\ell} |\mathrm{d}n| \tag{5}$$

where the first integral is over the physical distance ℓ along the propagation path. In the second integral, the OPL is expressed directly in terms of the effective refractive interfacial fluid thickness, which is $h_{n,\ell} = 1/|\nabla n|_\ell$ (Ref. 7). As usual, the refractive index is $n = c_0/c$, where c_0 is the speed of light in vacuum and c is the local speed of light. Because the velocity of light is related to the propagation

distance through $c = \mathrm{d}\ell/\mathrm{d}t$, we can also express the OPL integral as $\mathrm{OPL} = \int n\mathrm{d}\ell = c_0 \int (1/c)\,\mathrm{d}\ell = c_0 \int \mathrm{d}t$, that is, it follows that the OPL integral is essentially the integrated propagation time, or wavefront travel time, even though the integral is originally defined as a spatial integral.

In the present work, the emphasis is on the optical-wavefront structure. The optical wavefronts are physically the isosurfaces of the OPL, that is,

$$\mathrm{OPL}(\boldsymbol{x}, t) = \mathrm{const} \tag{6}$$

because, as just stated, the OPL integral can be interpreted as a propagation-time integral, that is, $(\mathrm{OPL})/c_0 = \int \mathrm{d}t$. A surface of constant OPL is, therefore, a surface on which all points have traveled over the same propagation time, that is, duration, and therefore this surface is the wavefront. By simply normalizing the OPL, one can see that the OPL integral is also essentially an optical-phase integral. We see, therefore, that isosurfaces of the OPL, or of the travel time, or of the optical phase, are all equivalent physical representations of the optical wavefronts. In contrast, the wavefront-location integral $\int c\mathrm{d}t = \int \mathrm{d}\ell$ does not of course have this property, that is, its isosurfaces do not represent the wavefronts, because the isosurfaces of the wavefront-location integral are just surfaces of constant propagation distance. This illustrates what is perhaps the most important physical property of the OPL integral, that is, that the OPL integral is physically and intuitively very helpful precisely because it has the property that the OPL isosurfaces are the wavefronts themselves.

In turbulent flows, and especially at large Reynolds numbers, the OPL isosurfaces or wavefronts can be expected to be highly irregular. In the present work, our objective is to characterize the physical structure of the optical wavefronts as a function of scale allowing for anisotropic scaling behavior. The first issue that needs to be addressed is that aero-optical wavefronts are physically highly anisotropic surfaces (compare Figs. 2 and 3). This is because, without any normalization, the spatial transverse extents of the optical wavefronts are in practice much larger than the OPL variations. This is especially so because the refractive-index variations, for example, as quantified by the rms magnitude, are relatively small when compared to unity for gas-phase flows. Consequently, as the integrals in Eq. (5) suggest, the OPL variations will be much smaller than the spatial transverse extent (i.e., aperture) of any optical beam in practice. The OPL variations are best expressed through the OPD, where

$$\mathrm{OPD} = \mathrm{OPL} - \int_{\mathrm{ray}} n_{\mathrm{ref}}(\boldsymbol{x}, t)\,\mathrm{d}\ell$$

where n_{ref} denotes a reference refractive index, for example, corresponding to a freestream condition. Physically, therefore, the wavefront anisotropy is present because

$$|\Delta n|_{\mathrm{rms}} \ll 1, \qquad \mathrm{OPD}_{\mathrm{rms}} \ll |\Delta\ell| \tag{7}$$

where $|\Delta n|_{\mathrm{rms}}$ and $\mathrm{OPD}_{\mathrm{rms}}$ denote, respectively, the rms magnitudes of the refractive-index variations and of the OPD of the distorted wavefront, and $|\Delta\ell|$ denotes a measure of the total optical-beam-propagation path, which is $|\Delta\ell| \sim L$ or $\lambda_{\max}$, that is, comparable to the large-scale extent L of the flow as far as the aero-optical interactions in the turbulent region are concerned. This strong anisotropy of aero-optical wavefronts refers to their physical, unnormalized structure. One can normalize the OPD so that the effective degree of anisotropy can change. By also scaling the spatial coordinates, one can examine the wavefronts at varying degrees of anisotropy, as will be shown next and in Sec. III.

The following ideas are applicable to both the wavefront surfaces and the OPL or OPD profiles. Taking the x and y directions as the spatial directions perpendicular to the incident-wavefront propagation direction, the OPD profiles are in this case functions of x and y as well as time, that is,

$$\mathrm{OPD}(x, y, t) \tag{8}$$

where, for simplicity of notation in what follows, x and y are the spatial coordinates normalized by the large-scale transverse extent L of the flow (compare Fig. 1), and OPD will denote the optical path difference normalized by $(\Delta n)_{\mathrm{ref}} L$ with $(\Delta n)_{\mathrm{ref}}$ denoting the reference (freestream-based) refractive-index difference. To be able to vary the anisotropy of the OPD, which will be needed in Secs. III and IV, we propose the use of scaling factors (stretching factors) for both the OPD and the spatial-extent coordinates, that is, so that the anisotropic transformation of the optical-wavefront surface can be represented as

$$\mathrm{OPD}(x, y, t) \rightarrow \alpha_{\mathrm{OPD}}\mathrm{OPD}(\alpha_x x, \alpha_y y, t) \tag{9}$$

where α_{OPD} is a scaling factor for the OPD and $\{\alpha_x, \alpha_y\}$ are scaling factors for the spatial-extent coordinates normal to the incident-wavefront propagation direction. These scaling factors can each be greater than or less than unity. For the example shown in Fig. 2, different values of α_{OPD} are employed for the same wavefront or OPD isosurface. We note, with regard to Eq. (9), that only two wavefront-anisotropy parameters are needed (only the ratios matter), and, therefore, we define a (vector) AWA parameter given by

$$\boldsymbol{\alpha} \equiv \{\alpha_{\mathrm{OPD}}/\alpha_x, \alpha_{\mathrm{OPD}}/\alpha_y\} \tag{10}$$

in terms of the ratios of the scaling factor of the OPD to each of the scaling factors of the transverse spatial coordinates. For a wavefront in two-dimensional space, such as in Fig. 3, only one scaling factor is needed; for example, the AWA parameter becomes $\alpha \equiv \alpha_{\mathrm{OPD}} / \alpha_x$. The proposed AWA parameter $\boldsymbol{\alpha}$ enables the variation of the effective anisotropy of aero-optical wavefronts, which can be used to examine their structure as a function of scale as will be shown in Secs. III and IV. The AWA parameter can be used not only in the study of the OPD isosurfaces but also in the study of the OPD field itself, if needed.

As already mentioned, the present anisotropy considerations are applicable to both the wavefront itself and to the OPL or OPD profiles. The proposed AWA parameter, therefore, is also applicable to both. In practice, it is important to appreciate that although the

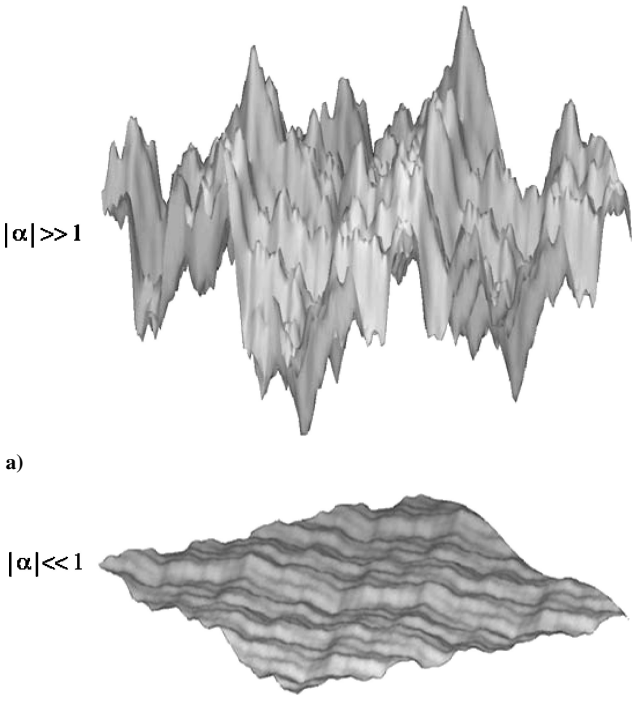

Fig. 2 Illustration of varying the effective anisotropy of an optical wavefront in three-dimensional space using the proposed AWA parameter α, [compare Eqs. (9) and (10)]. The same wavefront is shown with a) $|\alpha| \gg 1$ and with b) $|\alpha| \ll 1$.

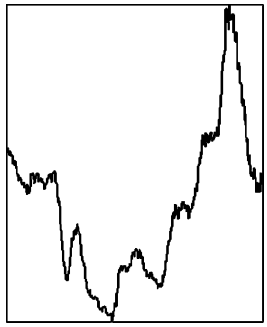

a)

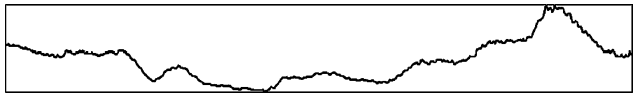

b)

Fig. 3 Example of an optical wavefront in two dimensions. The same wavefront is shown at two different values of the AWA parameter, which is a scalar-valued parameter in two dimensions and is $\alpha = \alpha_{\mathrm{OPD}}/\alpha_x$. In this example, the large-scale size of the wavefront bounding box is the same for each case, that is, $(\alpha_{\mathrm{OPD}}\ \alpha_x)^{1/2}$ is the same.

OPL isosurfaces represent the wavefronts, what is more straightforward to measure experimentally is the OPL or OPD profile, that is, the variation of the OPL in the reference measurement plane of a detector or along a reference line. It is helpful, however, to also appreciate that the OPL isosurfaces are, after all, derivable from the OPL field assuming the OPL field is known. For example, considering wavefronts that emerge from a turbulent shear flow and subsequently propagate in a near-field region of uniform reference refractive index, the wavefronts will propagate at a constant speed in the uniform-index region. As long as this region is in the near field, that is, without having to consider far-field propagation effects, the normalized OPL profiles are geometrically equivalent to the OPL isosurfaces. The preceding wavefront-anisotropy considerations, and the AWA parameter, are equally applicable to the profiles as well as isosurfaces of the OPL or OPD fields.

III. Anisotropic Box-Counting Technique for Characterization of Aero-Optical Wavefronts

To investigate the physical structure of optical wavefronts, a useful approach is to conduct box counting, which enables an examination of the manner in which the wavefronts' geometrical features vary with scale (e.g., Refs. 24 and 25). For each wavefront, a bounding box or rectangle is identified and partitioned successively into smaller boxes. The number of boxes containing the wavefront is counted at each box scale λ. This coverage count, denoted as $N_d(\lambda)$ in d dimensions, can be used to quantify the geometric structure as a function of scale. At the largest scale $\lambda_{\max}$, the coverage count is unity, that is, $N_d(\lambda_{\max}) = 1$. We sometimes also denote the largest scale as δ, that is, the bounding-box scale. One can normalize the coverage count by the total number of boxes available at each scale λ, and this is known as the coverage fraction

$$F_d(\lambda) = (\lambda/\lambda_{\max})^d N_d(\lambda) \tag{11}$$

where $0 \le F_d(\lambda) \le 1$ and the limiting values correspond to the smallest and largest scales, respectively. The physical meaning of the coverage fraction is that it is the geometric probability of finding a part of the wavefront in a λ-scale box. A larger value of $F_d(\lambda)$, at a given scale, indicates a more irregular wavefront structure at that scale.

Highly anisotropic behavior can be expected for aero-optical wavefronts (compare Sec. II) and, because of this, the scale λ must be treated as a vector in general, as was proposed for turbulent fluid interfaces in general by Catrakis.[26] In the present case

$$\boldsymbol{\lambda} = \{\lambda_{\mathrm{OPD}}, \lambda_x, \lambda_y\} \tag{12}$$

with the (scalar) box size λ denoting in the general case the magnitude of $\boldsymbol{\lambda}$. In three-dimensional space, for example, we can write this as

$$\lambda = \left(\lambda_{\mathrm{OPD}}\lambda_x\lambda_y\right)^{\frac{1}{3}} \tag{13}$$

where λ_{OPD} denotes the extent of each box along the OPD axis and $\{\lambda_x,\ \lambda_y\}$ denote the spatial extents of each box in the $\{x,\ y\}$ directions. The advantage of a scale magnitude defined as in Eq. (13) is that λ^3 can be identified as a volume occupied by each λ-sized box.

The most important quantity that the box-counting technique produces is the coverage dimension $D_d(\lambda)$ as a function of the scale magnitude λ. The coverage dimension can be computed as the fractional increase in the coverage count per unit fractional decrease in scale, or equivalently the logarithmic derivative of the coverage count with scale, that is,

$$D_d(\lambda) \equiv -\frac{\mathrm{d}N_d(\lambda)/N_d(\lambda)}{\mathrm{d}\lambda/\lambda} = -\frac{\mathrm{d}\log N_d(\lambda)}{\mathrm{d}\log\lambda} \tag{14}$$

and can be interpreted as a fractional (fractal) dimension whose departure from the topological dimension d_t of the wavefronts quantifies how complex the wavefront structure is.

The coverage dimension must be in the range

$$d_t \le D_d(\lambda) \le d \tag{15}$$

for optical wavefronts. In particular, at the smallest scales and largest scales respectively the coverage dimension reaches those limits, that is

$$D_d(\lambda) \to d_t \qquad \text{as} \qquad \lambda \to \lambda_{\min} \tag{16}$$

$$D_d(\lambda) \to d \qquad \text{as} \qquad \lambda \to \lambda_{\max} \tag{17}$$

For optical wavefronts in three dimensions, as indicated in Fig. 1, these limiting values become $d_t = 2$ and $d = 3$, respectively. For wavefronts in two dimensions (compare Fig. 3), these values become $d_t = 1$ and $d = 2$, respectively. It is also helpful to think of the relative coverage dimension of the wavefronts, that is, the coverage dimension relative to the topological dimension, which is given by $D_d(\lambda) - d_t$ in general, or $D_2(\lambda) - 1$ in two dimensions, for example. This is useful for comparing wavefront structure in different dimensions, for example, in three dimensions vs two dimensions, because the values of the relative coverage dimension must range from 0 to 1 independent of whether the wavefront is in a three- or two-dimensional region of the flow [compare Eq. (15)]. Recalling that at large Reynolds numbers one can expect similarity properties over a wide range of scales [compare Eq. (3)], another important use of the coverage dimension is that it can reveal such similarity properties, including the presence of self-similarity.

If the coverage dimension $D_d(\lambda)$ is a constant over a wide range of scales, then this would mean that the wavefront physically has scale-independent structure in that range of scales, and then the wavefront could be modeled using this self-similarity. Specifically, for self-similar behavior the coverage dimension would be $D_d(\lambda) = D_d = \text{const}$, and the structure of the wavefront could be extrapolated to larger Reynolds numbers [compare Eq. (2)] using

$$N_d(\lambda) \sim (\lambda_{\max}/\lambda)^{D_d} \tag{18}$$

over a range of scales $\lambda_{\min} \lesssim \lambda \lesssim \lambda_{\mathrm{LT}}$ [compare Eq. (3)]. The value of D_d would reflect the complexity of the wavefront structure that statistically repeats itself over a range of scales.

If, however, the coverage dimension is found to be a continuous function of scale throughout the range of scales, then the coverage count would no longer be a power law but instead would behave as

$$N_d(\lambda) = \exp\left\{\int_{\lambda}^{\lambda_{\max}} D_d(\lambda)' \frac{\mathrm{d}\lambda'}{\lambda'}\right\} \tag{19}$$

as can be readily seen by inverting Eq. (14). Such scale-dependent behavior, where for example the coverage dimension could be increasing with increasing scale over a range of scales, would mean that the complexity of the wavefront varies with scale. This would mean that more complicated, scale-dependent models would be needed to extrapolate the small-scale structure of optical wavefronts to larger Reynolds numbers. We note, however, that scale-dependent behavior on the basis of $D_d(\lambda)$ alone might not necessarily imply lack of self-similarity. Recent work has indicated that other scale-local measures might be needed to discern self-similar behavior in those cases where $D_d(\lambda)$ appears to be scale dependent.[12] In the cases, however, where there is clear evidence of scale independence in $D_d(\lambda)$, this quantity is sufficient to detect self-similarity.

As emphasized in Sec. II, aero-optical wavefronts can be expected to exhibit a strong anisotropy. A more general box-counting approach therefore is needed, to be useful for aero-optics, where one can examine the box-counting behavior of the wavefronts allowing for the possibility that they might be scale independent, that is, self-similar, in an anisotropic manner. Self-similar anisotropic behavior is sometimes also called self-affine behavior. Irregular self-affine objects exhibit structure that is scale independent but in a manner that depends on the direction. In other words, self-affine objects are anisotropically scale independent, whereas self-similar objects are isotropically scale independent.

We propose an anisotropic extension of the box-counting technique whereby the AWA parameter $\boldsymbol{\alpha}$ of Sec. II becomes a parameter in the coverage count and consequently in the coverage fraction as well as in the coverage dimension, that is,

$$N_d(\lambda; \boldsymbol{\alpha}) \qquad \text{and} \qquad F_d(\lambda; \boldsymbol{\alpha}) \tag{20}$$

with

$$D_d(\lambda; \boldsymbol{\alpha}) = -\frac{\mathrm{d} \log N_d(\lambda; \boldsymbol{\alpha})}{\mathrm{d} \log \lambda} \tag{21}$$

The introduction of the AWA parameter $\boldsymbol{\alpha}$ in the coverage quantities makes possible a practical examination of anisotropic structure. We note that an equivalent way to proceed would be to treat the scale λ as a vector $\boldsymbol{\lambda}$ [compare Eq. (12)] and then to define the coverage dimension through an extension of Eq. (14). This, however, would lead to coverage-dimension vectors expressed as partial derivatives of the coverage count. The proposed approach, that is, using the quantities in Eq. (21), offers instead a much simpler way to characterize the anisotropic structure of aero-optical wavefronts, with a coverage dimension that is scalar valued rather than vector valued.

As an example in two dimensions, Fig. 4 and 5 show the same optical wavefront at two different values of the AWA parameter $\boldsymbol{\alpha}$ with the boxes necessary to cover the wavefront in each case for several different scales. The corresponding coverage results are shown in Figs. 6a–6c. Note that the choice of the values of the AWA parameter, in Fig. 4 and 5, is such that they both have the same scale magnitudes, that is, the value of $(\alpha_{\mathrm{OPL}}\, \alpha_x)^{1/2}$ is the same for both examples. This was done so that any effects of the largest scales are removed in order to focus on the small-scale structures. Significantly, we see that for the same optical wavefront examined under different levels of anisotropy, different behavior is evident at the small scales in Fig. 6c. This is an important observation because it illustrates that this technique is sensitive to the presence of anisotropy at small scales, and, therefore, one can expect to be able to use it to examine aero-optical wavefronts at large Reynolds numbers as will be done in Sec. IV. It is also important to appreciate that the preceding ideas can be expected to be useful to examine not only the ensemble-averaged behavior of the instantaneous wavefronts but also the instantaneous wavefront structure itself. The latter is, of course, crucial in practical aero-optics applications.

IV. Scale-Local Structure of Aero-Optical Distortions at Large Reynolds Number and High Compressibility

In this section, we demonstrate the use of the proposed anisotropic box-counting technique for the characterization of the scale-local structure of aero-optical distortions. We are particularly interested in the behavior at large Reynolds numbers and high compressibility because this is a flow regime of practical interest in a number of aero-optics applications in high-speed flight, and also because previous work suggests that high-compressibility turbulent flows exhibit important differences at least at the large scales when compared to incompressible or weakly compressible turbulent flows (e.g., Refs. 27 and 28). Less is known about the effect of compressibility on the small-scale behavior at large Reynolds numbers. Computational results are available on compressible turbulent flows (e.g., Ref. 29) but are presently restricted to low Reynolds numbers. On the theoretical side, there are proposals of similarity and self-similarity properties at large Reynolds numbers (e.g., Ref. 11) that have been put forth for incompressible turbulence. However, it is presently not clear to what extent such incompressible-turbulence similarity properties are applicable at compressible-flow conditions including high compressibility.

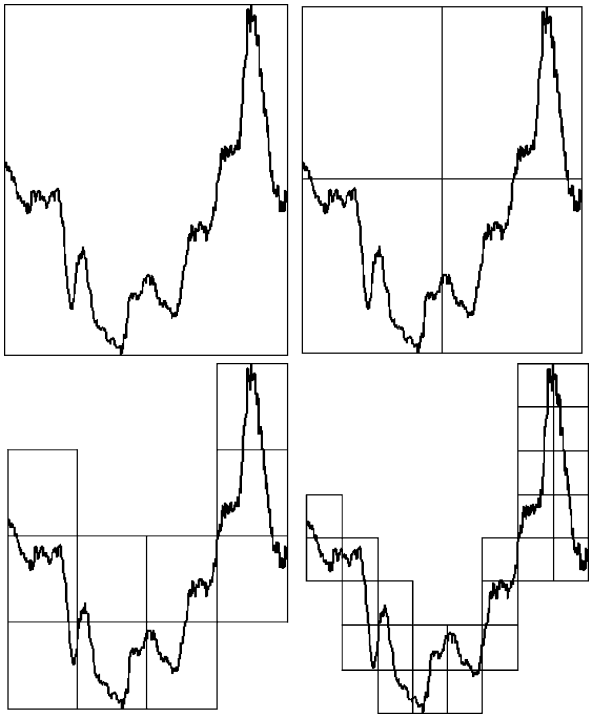

Fig. 4 Illustration of the anisotropic box-counting technique for the wavefront as shown in Fig. 3. Coverage boxes are shown at different scales. The coverage boxes are the boxes needed to completely contain the wavefront at each scale.

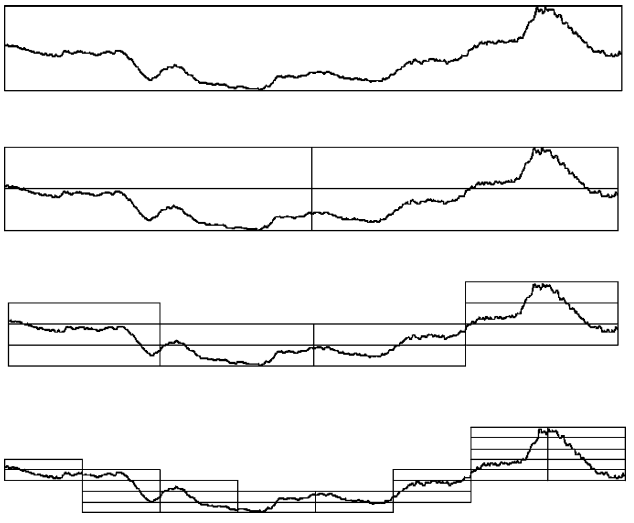

Fig. 5 Illustration of the anisotropic box-counting technique for the wavefront shown in Fig. 3.

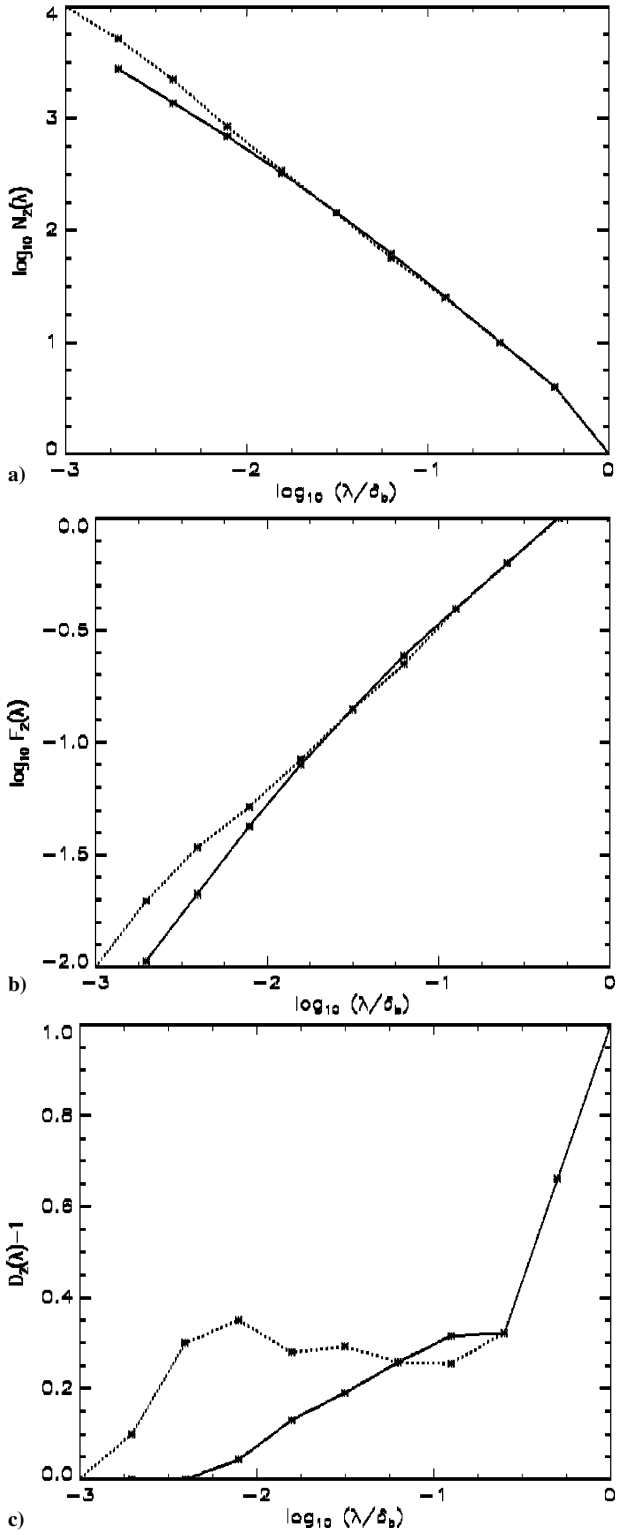

Fig. 6 Comparison of the coverage count, coverage fraction, and coverage dimension for the wavefront from Fig. 3. The dotted curves correspond to Fig. 3a, and the solid curves correspond to Fig. 3b. The differences at the small scales indicate that the small-scale behavior is sensitive to the choice of the AWA parameter.

To examine the applicability of the technique proposed in Secs. II and III, we employ recent wavefront data derived from experimental studies of aero-optical distortions in high-compressibility shear layers between different gases.[5] A discussion of the experimental technique can be found in the companion paper[7] with a more complete description in Ref. 5. The aero-optical behavior in these measurements is dominated by mixing effects. The important issue of mixing vs density effects in aero-optics is discussed

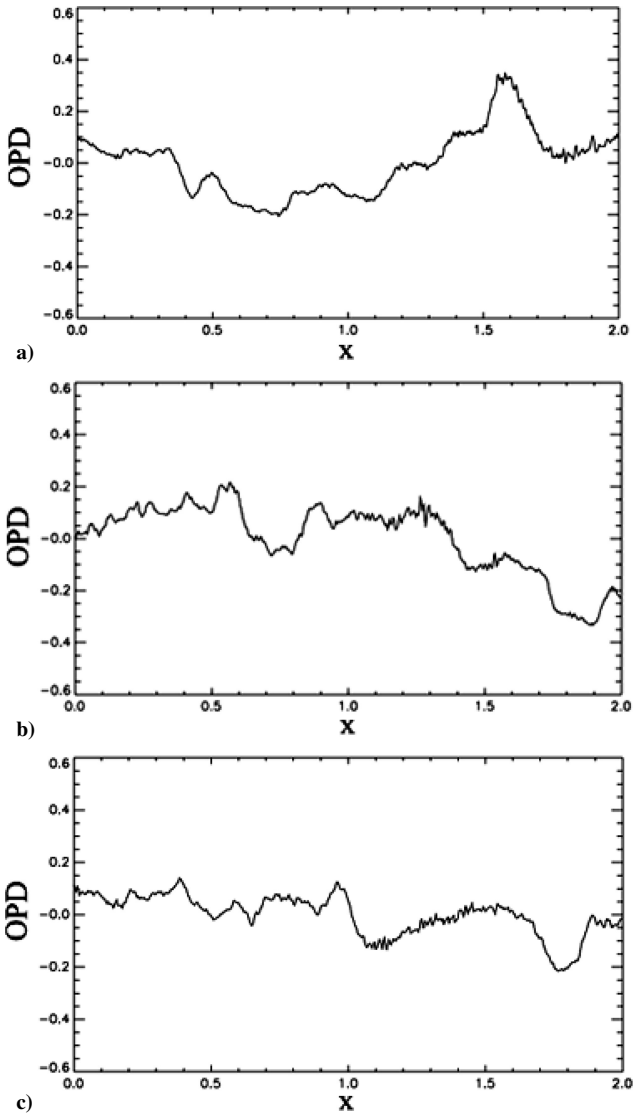

Fig. 7 Examples of experimental wavefront OPD profiles, OPD(x), derived from two-dimensional refractive-index field measurements in large-Reynolds-number ($Re \sim 10^6$), high-compressibility ($M_c \sim 1$) shear layers between dissimilar gases.[5,7] The OPD and spatial coordinate x denote normalized values. The normalization employs the transverse spatial extent of the shear layer and the ambient (freestream) refractive-index difference. The incident wavefronts are initially linear, that is, straight, and propagate transverse to the flow, from one freestream to the other, through two-dimensional spatial streamwise slices of the flow. The wavefront OPD profiles correspond to the aero-optical wavefronts that emerge from the turbulent flow region.

in Jumper and Fitzgerald[6] and also in the companion article to the present work.[7] For the data employed here, a large-scale Reynolds number of $Re \sim 10^6$ and a convective Mach number of $M_c \sim 1$ were achieved, and the OPD profiles corresponding to wavefronts emerging normal to the shear layers were derived by Fourier filtering the refractive-index field, as described in Dimotakis et al.[5] Examples of the OPD profiles at the high-compressibility flow conditions are shown in Figs. 7a–7c. The optical-wavefront distortions correspond to the aero-optical interactions in a two-dimensional plane transverse to the shear layer. The incident wavefronts are initially linear, that is, straight, and subsequently propagate transverse to the flow, from one freestream to the other, through two dimensional spatial streamwise slices of the flow. The wavefront OPD profiles correspond to the aero-optical wavefronts that emerge from the turbulent flow region. Although the wavefront data in Figs. 7a–7c are not fully resolved, the resolution is sufficient to capture a large fraction of the full range of scales at these large Reynolds numbers. This fraction

of the range of scales is estimated to be $\sim 500{:}1$ based on the camera pixel resolution that was employed to record the flow images from which the OPD profiles were derived. Keeping in mind that similarity properties are not expected throughout the entire range of scales smaller than the large scale, but rather in a fraction of those scales [compare Eq. (3)], these data can be expected to be useful to examine the presence of similarity or self-similarity in the wavefront structure.

For the shear-layer data, the OPD profiles are functions of the streamwise coordinate x normalized by the transverse extent L of the large-scale shear in this flow, that is,

$$\mathrm{OPD}(x/L) \tag{22}$$

The incident wavefronts are assumed to be planar (linear in the planar slice of the flow studied) so that the coverage dimension is

$$D_2(\lambda) = 1 \tag{23}$$

prior to propagation of the wavefronts through the shear layer. Subsequent to propagation and distortion of the wavefronts, the relevant AWA parameter associated with the OPD profile is

$$\alpha \equiv \alpha_{\mathrm{OPD}}/\alpha_x \tag{24}$$

[compare Sec. II and Eqs. (9) and (10)] corresponding to the two-parameter stretched-OPD profile, that is,

$$\alpha_{\mathrm{OPD}}\mathrm{OPD}[\alpha_x(x/L)] \tag{25}$$

As pointed out in Sec. II, the two parameters α_{OPD} and α_x are equivalent to the single AWA parameter $\alpha = \alpha_{\mathrm{OPD}} / \alpha_x$. One parameter is sufficient, for wavefronts in two-dimensional space, to permit an examination of the wavefront structure at different levels of anisotropy.

Box counting was performed on the high-compressibility shear-layer wavefront profiles for several different values of the AWA parameter α, over the range $0.3 \lesssim \alpha \lesssim 3$, that is, spanning one order of magnitude in the AWA parameter. For each value of α, the wavefront was stretched and subsequently partitioned into boxes (tiles in two dimensions) so that the box count was computed as a function of scale, that is,

$$N_2(\lambda; \alpha) \tag{26}$$

where the subscript 2 denotes that these data are spatially two dimensional. From the coverage count, we computed the coverage fraction and the coverage dimension as a function of scale, that is,

$$F_2(\lambda; \alpha) = (\lambda/\lambda_{\max})^2 N_2(\lambda; \alpha) \tag{27}$$

$$D_2(\lambda; \alpha) = -\frac{\mathrm{d}\log N_2(\lambda; \alpha)}{\mathrm{d}\log \lambda} \tag{28}$$

Two important observations were made:

1) The small-scale wavefront behavior depends strongly on the AWA parameter α.

2) There exists a particular value of the AWA parameter $\alpha = \alpha^*$ for which the small-scale wavefront structure is found to be scale independent over a range of scales.

The first observation confirms the idea in Sec. II that aero-optical wavefronts are highly anisotropic and shows that the technique described in Sec. III is capable of detecting the dependence of the small-scale structure on this anisotropy. The second observation, that is, that there is scale independence over a range of scales for a particular value α^*, which is found to be $\alpha^* \simeq 0.9$ for the present data, is particularly important. The results are shown in Figs. 8a–8c, which depict respectively the coverage count $N_2(\lambda; \alpha^*)$, coverage fraction $F_2(\lambda; \alpha^*)$, and the relative coverage dimension $D_2(\lambda; \alpha^*) - 1$ for the critical value of the AWA parameter. For values of α smaller than or greater than α^*, qualitatively different behavior was observed:

1) For $\alpha < \alpha^*$, the wavefront structure is scale dependent with relatively smaller values of the coverage dimension at intermediate scales.

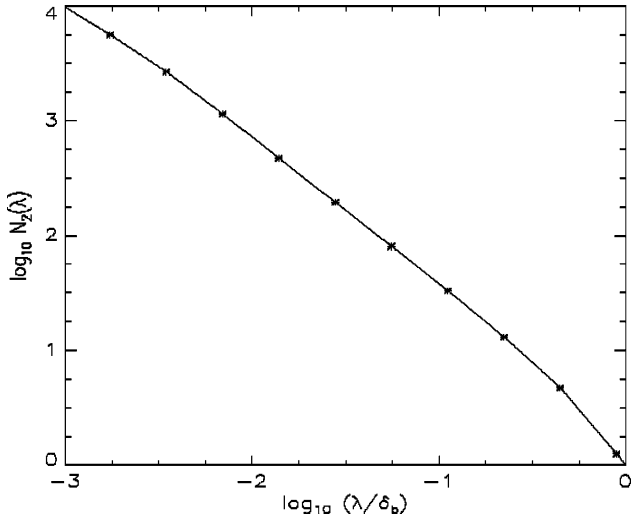

a)

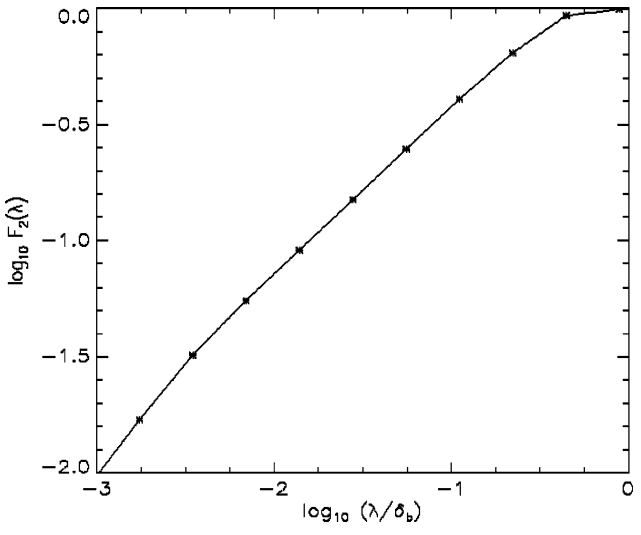

b)

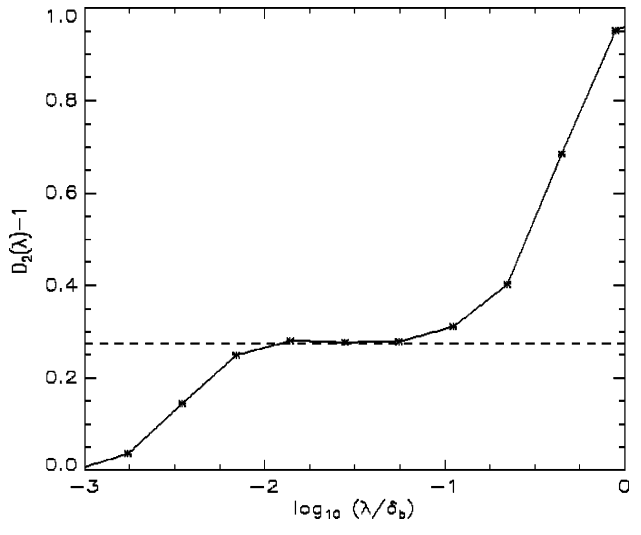

c)

Fig. 8 Ensemble-averaged results for the instantaneous structure of wavefront OPD profiles in large-Reynolds-number ($Re \sim 10^6$), high-compressibility ($M_c \sim 1$) shear layers (compare Figs. 7a–7c): a) coverage function $N_2(\lambda; \alpha^*)$, b) coverage fraction $F_2(\lambda; \alpha^*)$, and c) relative coverage dimension $D_2(\lambda; \alpha^*) - 1$. The value of the critical AWA parameter α^* for the results shown is $\alpha^* \sim 0.9$. The plateau in c) indicates a clear presence of self-similarity of the anisotropic wavefront structure over a range of small scales spanning nearly a decade.

2) There exists a particular value of the AWA parameter $\alpha = \alpha^*$ for which the small-scale wavefront structure is found to be scale independent over a range of intermediate scales.

3) For $\alpha > \alpha^*$, the wavefront structure is scale dependent with relatively larger values of the coverage dimension at intermediate scales.

The significance of the observed behavior at $\alpha = \alpha^*$ is that this shows the presence of an intermediate range of small scales in which the wavefront is self-similar, that is, a range of scales in which the coverage dimension is nearly a constant:

$$D_2(\lambda; \alpha^*) \simeq \text{const} \simeq 1.27 \tag{29}$$

The uncertainty in the coverage dimension is estimated to be ± 0.025, estimated from the variations between individual realizations. The $D_2 \simeq 1.27$ value is found for the present flow conditions of high compressibility and large Reynolds number. At other flow conditions, for example, different compressibility or Reynolds numbers, it can exhibit a dependence, but this would be expected to be a weak dependence as long as the flow is fully developed. The $D_2 \simeq 1.27$ value is lower than the $D_2 \simeq 1.35$ value reported for incompressible flows (e.g., Ref. 11), and this is consistent with expectations that the dimension should decrease with increasing compressibility (e.g., Ref. 20).

This finding can be expected to be useful in order to extrapolate the behavior to even larger Reynolds numbers at high compressibility, at least in shear layers, using

$$N_2(\lambda; \alpha^*) \sim (\lambda_{\max}/\lambda)^{1.27} \tag{30}$$

[compare Eq. (18)] because the exponent already corresponds to large-Reynolds-number flow conditions. From Fig. 8c, we see that the self-similar behavior is evident in the measurements over a range of scales that span approximately one decade. Even though the Reynolds number associated with the shear layer is large, that is, $Re \sim 10^6$, and corresponds to a full range of flow scales given by $\lambda_{\max}/\lambda_{\min} = Re^{3/4} \sim 3 \times 10^4$, the range of scales over which similarity is expected is smaller. For example, a conservative estimate[13] is the ratio of the Liepmann–Taylor scale λ_{LT} to the Kolmogorov scale λ_K, which grows slowly with Reynolds number, specifically $\lambda_{\text{LT}}/\lambda_{\text{K}} \sim Re^{1/4} \sim 30$ [compare Eqs. (2) and (3) in Sec. II]. This estimate, at least of the extent of the range of self-similar scales, is closer to the presently observed behavior (compare Fig. 8c). Higher-resolution measurements would be needed to discern this issue further, that is, whether the range of scales exhibiting self-similar behavior extends to smaller scales yet. We note that the critical value α^* of the AWA parameter might depend to some extent on the Reynolds number and/or Mach number, and possibly on the flow boundary conditions. However, as long as the Reynolds number is large, that is, meets the criterion for fully developed turbulence (compare Sec. II), one can expect that the small-scale structure of the wavefronts and the critical value of the AWA parameter will be at most weakly dependent on these flow parameters. This is because the small-scale structure at large Reynolds numbers is at most weakly sensitive to the large-scale behavior (e.g., Refs. 11 and 13 and references therein).

The present finding of scale independence of the small-scale optical-wavefront structure over a range of scales at high compressibility provides experimental evidence that self-similarity is present in aero-optical interactions at high-compressibility flow conditions. Computational studies of compressible flows at low Reynolds numbers have indicated inertial-range scaling based on power spectra (e.g., Ref. 29), and this supports the present finding of self-similarity, although spectral behavior alone cannot be related uniquely to the physical structure of the fluid interfaces. The present observation of self-similar behavior in the physical structure of the distorted aero-optical wavefronts indicates that turbulent fluid interfaces at high compressibility also possess self-similarity properties. Self-similar behavior of the fluid interfaces would be sufficient to explain the observed self-similar aero-optical behavior, with anisotropy inherent in the wavefront OPD (compare Sec. II). Quantification and modeling of the physical structure of optical wavefronts, in real space as opposed to Fourier space, requires tools such as the technique presently demonstrated. The present results demonstrate that optical-wavefront self-similarity can be detected with the proposed approach using the AWA parameter. The present results demonstrate that optical-wavefront self-similarity can be detected with the proposed approach using the AWA parameter. This capability provides a key ingredient useful for various aero-optical applications (e.g., Refs. 30–37).

V. Conclusions

The proposed method of anisotropic box counting provides a technique useful for the scale-local characterization of the physical structure of aero-optical wavefronts, that is, as a function of scale. The aero-optical-wavefront-anisotropy (AWA) parameter, defined as a ratio of scaling factors for the wavefront distortions and for the transverse extent of the wavefronts, combined with an anisotropic generalization of box counting enables a scale-local examination of wavefronts at varying degrees of anisotropy. This is particularly useful for the study of aero-optical wavefronts at large Reynolds numbers. Demonstration of this technique to experimental data in large-Reynolds-number ($Re \sim 10^6$), high-compressibility ($M_c \sim 1$) turbulent shear layers shows the presence of anisotropic self-similarity, or self-affinity, in the wavefront structure over a range of small scales spanning nearly a decade, as detected by varying the AWA parameter and conducting a scale-local examination of the distortions. Even though the data employed in this study are dominated by mixing effects as opposed to solely density effects, the anisotropy considerations and the AWA parameter can be expected to be useful in both cases.

The present finding and technique have helpful consequences for large-Reynolds-number experimental studies as well as modeling and computational studies. The data show the utility of the technique to detect scaling in large-Reynolds-number flow experiments using the optical behavior and as such suggest an optical means to probe aspects of the mixing behavior at large Reynolds numbers. The present finding also provides a means to extrapolate the small-scale structure of optical distortions at high compressibility to larger Reynolds numbers. This can be expected to be useful in efforts to develop computational models and simulations of optical behavior in flows at practical flight conditions with large Reynolds numbers (e.g., Refs. 9 and 30–33) . The present self-similarity model of the wavefront distortions suggests a key ingredient to help construct effective subgrid-scale models in large-eddy simulations of aero-optical interactions. Small-scale properties of high-compressibility flows are also valuable because they can be coupled with descriptions that address the large-scale behavior of high-compressibility flows (e.g., the companion paper by Catrakis and Aguirre[7]) in order to develop frameworks that are capable of describing the behavior across the entire range of scales. Furthermore, this can provide the means to compare the cumulative effects of distortions at small scales to the effects at the large scales. These implications can be expected to be especially pertinent in applications that require high-resolution optical imaging (e.g., Ref. 34), long-range high-energy-laser beam propagation (e.g., Refs. 35 and 36), or free-space laser communications (e.g., Refs. 1 and 37).

Acknowledgments

This work is supported by the Air Force Office of Scientific Research through Grant F49620-02-1-0142 (Thomas Beutner, Program Manager) and is part of a program on aero-optical interactions in turbulent flows. The authors are grateful to Eric Jumper for his guidance and advice on the present work and to Paul Dimotakis for his contributions to earlier related work. The authors are also grateful to Jonathan Mason and Jennifer Nathman for their assistance with this paper as well as to the reviewers for their insightful comments.

References

[1] Andrews, L. C., Phillips, R. L., and Hopen, C. Y., *Laser Beam Scintillation with Applications*, SPIE Optical Engineering Press, 2001.

[2]Kyrazis, D., "Optical Degradation by Turbulent Free Shear Layers," *Optical Diagnostics in Fluid and Thermal Flow*, edited by S. S. Cha and J. D. Trolinger, Society of Photo-Optical Instrumentation Engineers, Bellingham, WA, 1993, pp. 170–181.

[3]Fitzgerald, E. J., and Jumper, E. J., "Further Consideration of Compressibility Effects on Shear-Layer Optical Distortion," AIAA Paper 99-3617, June 1999.

[4]Fitzgerald, E. J., and Jumper, E. J., "The Optical Distortion Mechanism in a Nearly Incompressible, Free Shear Layer," *Journal of Fluid Mechanics*, Vol. 512, 2004, pp. 153–189.

[5]Dimotakis, P. E., Catrakis, H. J., and Fourguette, D. C. L., "Flow Structure and Optical Beam Propagation in High-Reynolds-Number Gas-Phase Shear Layers and Jets," *Journal of Fluid Mechanics*, Vol. 433, 2001, pp. 105–134.

[6]Jumper, E. J., and Fitzgerald, E. J., "Recent Advances in Aero-Optics," *Progress Aerospace Sciences*, Vol. 37, 2001, pp. 299–339.

[7]Catrakis, H. J., and Aguirre, R. C., "New Interfacial Fluid Thickness Approach in Aero-Optics with Applications to Compressible Turbulence," *AIAA Journal*, Vol. 42, No. 10, 2004, pp. 1973–1981.

[8]Gilbert, K. G., and Otten, L. J., *Aero-Optical Phenomena*, Vol. 80, Progress in Astronautics and Aeronautics, AIAA, New York, 1982.

[9]Truman, C. R., and Lee, M. J., "Effects of Organized Turbulence Structures on the Phase Distortion in a Coherent Optical Beam Propagating Through a Turbulent Shear Flow," *Physics of Fluids A*, Vol. 2, 1990, pp. 851–857.

[10]Chew, L., and Christiansen, W., "Coherent Structure Effects on Optical Performance of Plane Shear Layers," *AIAA Journal*, Vol. 29, 1991, pp. 76–80.

[11]Sreenivasan, K. R., "Fractals and Multifractals in Fluid Turbulence," *Annual Review Fluid Mechanics*, Vol. 23, 1991, pp. 539–600.

[12]Catrakis, H. J., Aguirre, R. C., and Ruiz-Plancarte, J., "Area–Volume Properties of Fluid Interfaces in Turbulence: Scale-Local Self-Similarity and Cumulative Scale Dependence," *Journal of Fluid Mechanics*, Vol. 462, 2002, pp. 245–254.

[13]Dimotakis, P. E., "The Mixing Transition in Turbulent Flows," *Journal of Fluid Mechanics*, Vol. 409, 2000, pp. 69–98.

[14]Catrakis, H. J., "Turbulence and the Dynamics of Fluid Interfaces with Applications to Mixing and Aero-Optics," *Recent Research Developments in Fluid Dynamics*, edited by N. Ashgriz and R. Anthony, Transworld Research Network, Kerala, India, 2004.

[15]Villermaux, E., and Innocenti, C., "On the Geometry of Turbulent Mixing," *Journal of Fluid Mechanics*, Vol. 393, 1999, pp. 123–147.

[16]Catrakis, H. J., and Dimotakis, P. E., "Mixing in Turbulent Jets: Scalar Measures and Isosurface Geometry," *Journal of Fluid Mechanics*, Vol. 317, 1996, pp. 369–406.

[17]Hentschel, H. G. E., and Procaccia, I., "Passive Scalar Fluctuations in Intermittent Turbulence with Applications to Wave Propagation," *Physical Review A*, Vol. 28, 1983, pp. 417–426.

[18]Schwartz, C., Baum, G., and Ribak, E. N., "Fractal Character of Turbulence-Degraded Wavefronts," *8th Meeting on Optical Engineering and Remote Sensing, SPIE Proceedings*, Vol. 1971, Society of Photo-Optical Instrumentation Engineers, Bellingham, WA, 1993, pp. 476–485.

[19]Schwartz, C., Baum, G., and Ribak, E. N., "Turbulence-Degraded Wave Fronts as Fractal Surfaces," *Journal of the Optical Society America*, Vol. 11, No. 1, 1994, pp. 444–451.

[20]Smits, A. J., and Dussauge, J.-P., *Turbulent Shear Layers in Supersonic Flow*, AIP Press, Woodbury, NY, 1996.

[21]Poggie, J., "Quantitative Flow Visualization Applied to the Study of Compressible Turbulent Flow," M.S. Thesis, Princeton Univ., Princeton, NJ, 1991.

[22]Kolmogorov, A. N., "The Local Structure of Turbulence in Incompressible Viscous Fluid for Very Large Reynolds Numbers," *Doklady Akademii Nauka SSSR*, Vol. 30, 1941, pp. 301–305.

[23]Andrews, L. C., and Phillips, R. L., *Laser Beam Propagation Through Random Media*, SPIE Optical Engineering Press, Bellingham, WA, 1998.

[24]Catrakis, H. J., Aguirre, R. C., Thayne, R. D., McDonald, B. A., and Hearn, J. W., "Are Turbulence-Degraded Optical Wavefronts and Beam Trajectories Fractal?" AIAA Paper 2001-2801, June 2001.

[25]Catrakis, H. J., and Aguirre, R. C., "Inner-Scale Structure of Turbulence-Degraded Optical Wavefronts," AIAA Paper 2002-2269, June 2002.

[26]Catrakis, H. J., "Distribution of Scales in Turbulence," *Physical Review E*, Vol. 62, 2000, pp. 564–578.

[27]Samimy, M., and Elliot, G. S., "Effects of Compressibility on the Characteristics of Free Shear Layers," *AIAA Journal*, Vol. 28, 1990, pp. 439–445.

[28]Papamoschou, D., "Structure of the Compressible Turbulent Shear Layer," *AIAA Journal*, Vol. 29, 1991, pp. 680, 681.

[29]Porter, D. H., Woodward, P. R., and Pouquet, A., "Inertial Range Structures in Decaying Compressible Turbulent Flows," *Physics of Fluids*, Vol. 10, 1998, pp. 237–245.

[30]Elghobashi, S. E., and Wassel, A. T., "The Effect of Turbulent Heat Transfer on the Propagation of an Optical Beam Across Supersonic Boundary/Shear Layers," *International Journal of Heat and Mass Transfer*, Vol. 23, 1980, pp. 1229–1241.

[31]Tsai, Y.-P., and Christiansen, W. H., "Two-Dimensional Numerical Simulation of Shear Layer Optics," *AIAA Journal*, Vol. 28, 1990, p. 2092.

[32]Mani, A., Wang, M., and Moin, P., "Computation of Optical Beam Propagation Through Numerically Simulated Turbulence," *Bulletin of the American Physical Society*, 2003.

[33]Jones, M., and Bender, E. E., "CFD-Based Computer Simulation of Optical Turbulence Through Aircraft Flowfields and Wakes," AIAA Paper 2001-2798, June 2001.

[34]Kern, B., Dimotakis, P., Lang, D., and Martin, C., "Aberrating Medium Characterization and Image Reconstruction with a Quadrature-Phase Interferometer," AIAA Paper 2003-3610, June 2003.

[35]Fleck, J. A., Jr., Morris, J. R., and Feit, M. D., "Time-Dependent Propagation of High Energy Laser Beams Through the Atmosphere," *Applied Physics*, Vol. 10, 1976, pp. 129–160.

[36]Yahel, R. Z., "Turbulence Effects on High Energy Laser Beam Propagation in the Atmosphere," *Applied Optics*, Vol. 29, 1990, pp. 3088–3095.

[37]Gordeyev, S., Jumper, E. J., Ng, T. T., and Cain, A. B., "Aerooptical Characteristics of Compressible, Subsonic Turbulent Boundary Layers," AIAA Paper 2003-3606, June 2003.

H. Atassi
Associate Editor